Study of ω production near threshold in the reaction $\pi^- p \to \omega n$

J. Keyne, D. M. Binnie, J. Carr, N. C. Debenham, A. Duane, D. A. Garbutt, W. G. Jones, and I. Siotis
Department of Physics, Imperial College, London, United Kingdom

J. G. McEwen
Department of Physics, Southampton University, Southampton, United Kingdom
(Received 17 February 1976)

We have investigated ω production in the reaction $\pi^- p \to \omega n$ very close to threshold. The dependence of the mass, width, branching ratio, and cross section upon the final-state c.m. momentum, P^*, were studied. The mass and width were independent of P^* with values of 782.4 ± 0.5 and 10.22 ± 0.43 MeV, respectively. The branching ratio $\Gamma(\omega \to \pi^0\gamma)/\Gamma(\omega \to \pi^+\pi^-\pi^0)$ was also constant, having a value of 0.084 ± 0.013. An upper limit of 0.18 was set on the branching ratio $\Gamma(\omega \to \pi^0\pi^0\gamma)/\Gamma(\omega \to \pi^0\gamma)$. We observed a rapid fall in the cross section below $P^* = 100$ MeV/c. This could not be explained in terms of S-wave production alone, but could be fitted by a resonant P wave plus a noninterfering S wave.

I. INTRODUCTION

In a recent paper,[1] we presented results on the η, ω, X^0, and ϕ mesons obtained at incident momenta within a few MeV/c of their thresholds in the reaction $\pi^- + p \to$ missing mass $+ n$. By defining the momentum of the final-state neutron using a time-of-flight technique and scanning through a small range of the initial-pion momentum, we were able to measure the production cross section, σ, down to very low values of the final-state c.m. momentum, P^*. In this region there is an *a priori* expectation that S waves will dominate and that σ/P^* will be constant. This was indeed found for η production. However, our results for ω production showed a striking fall in σ/P^* at very low P^*.

In this paper, we report the results of a new experiment using the same technique and designed to investigate in detail the ω meson as produced near threshold. A further aim of the experiment was to make a precision measurement of the ω mass and width. The main requirement of the new experiment was therefore increased statistical precision with the apparatus essentially unchanged. However, because of the nonzero angle subtended to the beam by the ring of six neutron counters, there was a lower limit to P^* for detected events of about 30 MeV/c. A second run was therefore made with a single neutron counter in the beam, i.e., including zero degrees. For a study of the behavior of the ω with P^* these two runs were combined. For the precise measurement of the ω mass and width, only data from the ring of six neutron counters were used. The experiment was carried out at the Rutherford Laboratory using the proton synchroton NIMROD.

II. TECHNIQUE

The apparatus is shown in Fig. 1. A π^- beam of precisely determined momentum was incident on a 29.4-cm-long hydrogen target. Neutrons were detected at a mean angle of 2.8° by a ring of 6 neutron counters 6.15 m downstream from the target. Each counter consisted of a cylinder of plastic scintillator, 30 cm in both diameter and length, and had a neutron detection efficiency of about 25%.

An additional set of data was obtained with the six neutron counters, $N_{1\text{-}6}$, replaced by a single counter, N_7, on the beam axis, 4.15 m downstream of the target. The two sets of data are referred to as $N_{1\text{-}6}$ and N_7, respectively.

The target was surrounded by an array of scintillation counters (identical with that described in Ref. 1) referred to as the decay array. The polar region 11°–132° was covered by an inner set of 20 counters to detect charged particles and an outer set of 40, consisting of lead-scintillator sandwiches, to detect γ rays. These two sets of counters defined azimuthal bins of 18°. In addition, charged particles could also be detected in the polar regions 5°–11° and 132°–165°. The detection efficiency of the counters for charged particles was >99% and for γ rays it was ~90% for γ energies >100 MeV. This array of counters was used off-line to select $\pi^+\pi^-\pi^0, \pi^0\gamma$, etc. final states and hence to measure the ω branching ratios.

The kinematics for a neutron angle corresponding to the $N_{1\text{-}6}$ ring of counters are illustrated in Fig. 2, which shows lines of constant missing mass on a plot of P_π, the beam momentum, versus τ, the neutron time of flight minus the time of flight of beam pions over 6.15 m. Since the c.m. momentum

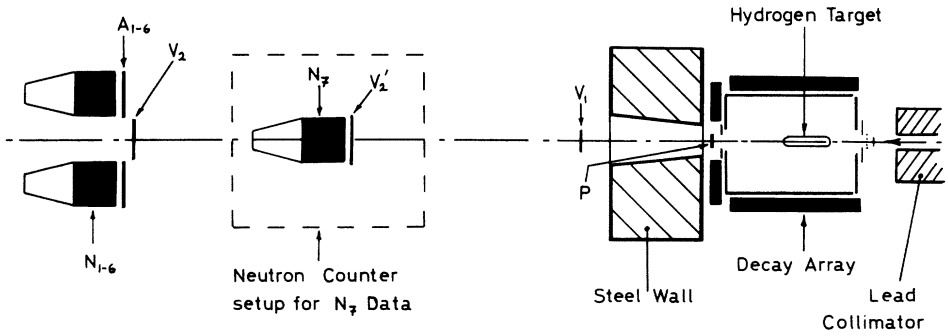

FIG. 1. (Not drawn to scale.) The general layout, excluding the beam. Incident π^- mesons enter from the right and either interact in the hydrogen target or are vetoed by counters $V1$ and $V2$. Neutrons and protons produced at a small angle (1.4–4.2°) may enter one of the six cylindrical neutron counters N_{1-6} and are distinguished by counters A_{1-6} and counter P. Secondary mesons and γ rays are detected by 66 counters surrounding the hydrogen target. For the detection of neutrons produced at zero degrees the neutron counters N_{1-6} were replaced by a neutron counter on the beam axis, N_7, as shown.

P^* is just the Lorentz transform of the neutron laboratory momentum, it can be defined without reference to the missing mass and in Fig. 2 we also show lines of constant P^*. Along the constant P^* lines the missing mass, m_3, varies linearly with P_π to a very good approximation. Note that the four-momentum transfer squared, t, is a function only of the neutron time of flight. The kinematics for the N_7 data are essentially the same except that P^* is lower.

The number of events falling within a certain range of P^* is proportional to $d^2\sigma/dt\,dm_3$ times a Jacobian which is a slowly varying function of P_π (varying typically by 1.5%/10 MeV/c). Hence by counting the number of events falling within a fixed range of P^*, normalized to a constant number of beam pions, as a function of beam momentum, one obtains a plot of $d^2\sigma/dt\,dm_3$ against a linear mass scale. We refer to such plots as yield curves. Figure 3 shows yield curves for fixed P^* intervals around the ω threshold. As can be seen from Fig. 2, over the width of the ω fixed P^* is essentially equivalent to fixed t. Hence the shape of the ω resonance as manifested in a yield curve will be

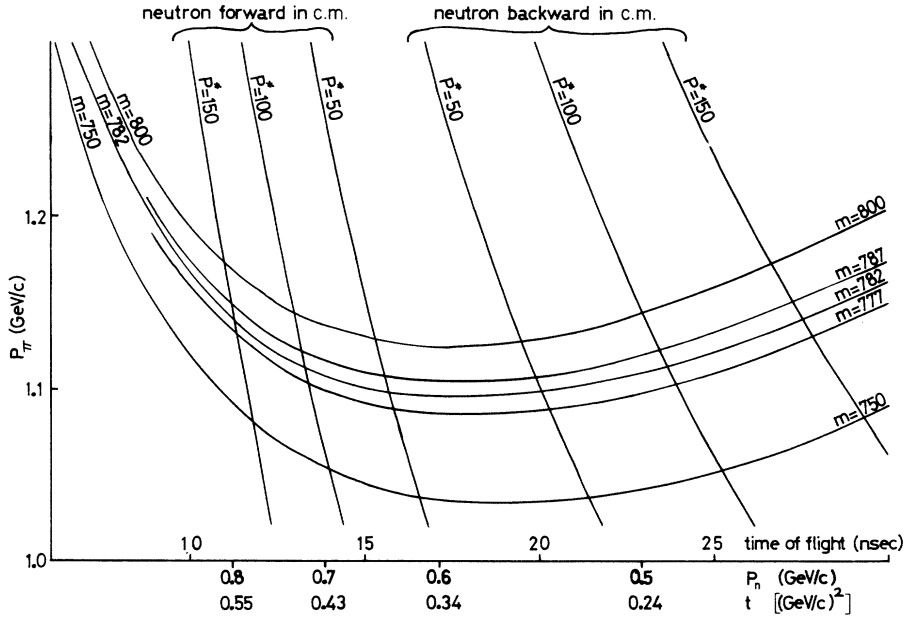

FIG. 2. The kinematics for N_{1-6}. The relationship between P_π and τ at $\theta_n = 2.8°$ for various values of missing mass, m, in MeV and c.m. momentum, P^*, in MeV/c is shown. Note also the neutron momentum, P_n, and four-momentum transfer, t, scales.

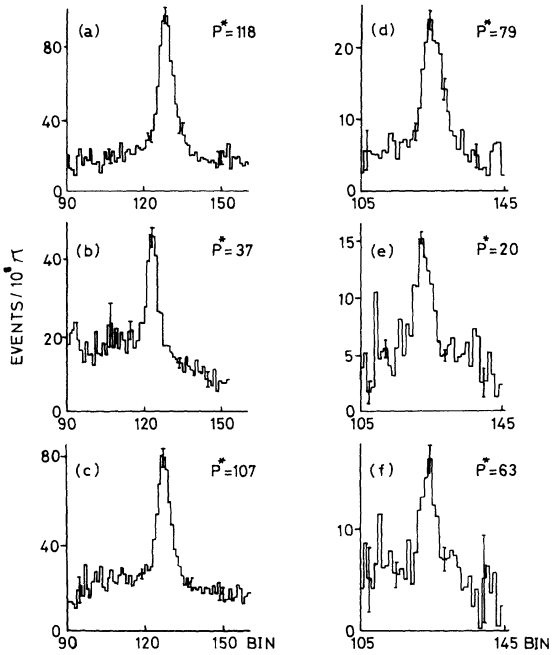

FIG. 3. Yield curves for narrow P^* intervals from N_{1-6} (a)–(c) and N_7 (d)–(f). In (a), (d), (b), (e), and (c), (f) the neutrons are traveling forward, nearly at rest, and backward in the c.m., respectively. The P^* values shown (in MeV/c) correspond to the peak of the P^* distribution.

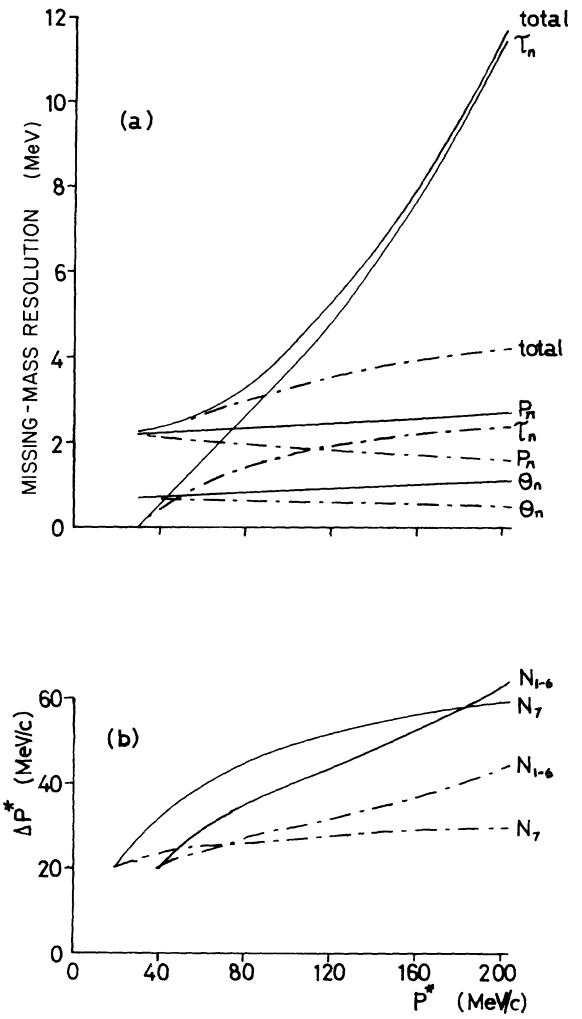

FIG. 4. (a) The missing-mass resolution (standard deviation) and its component contributions as a function of P^* for N_{1-6}. (b) The P^* resolution (FWHM) as a function of P^* for N_{1-6} and N_7. The solid and dashed lines correspond to neutrons traveling forward and backward in the c.m., respectively.

insensitive to the t or P^* behavior of its production cross section.

The area under the resonance signal gives the value of $d\sigma/dt$ averaged over the P^* interval specified. If the production angular distribution is isotropic, then the total cross section σ is related to $d\sigma/dt$ by $\sigma = 4P^*K^*(d\sigma/dt)$, where K^* is the initial-state c.m. momentum. Thus, in this circumstance, the value of $d\sigma/dt$ determines the ratio σ/P^*.

The missing-mass resolution of the N_{1-6} data is shown as a function of P^* in Fig. 4(a) together with the component contributions. Since the neutron counters were positioned near 0° the contribution from uncertainty in the neutron recoil angle (±1.4°) was small. The timing contribution corresponded to a Gaussian-shaped error with a standard deviation of 0.6 nsec. At low P^* the missing-mass resolution was dominated by the uncertainty in the beam pion momentum. This had two components. Scintillation-counter hodoscopes positioned at the focal planes of the spectrometer-defined momentum bins which had a triangular profile of full width at half maximum (FWHM) 0.5%. In addition, the beam pions lost up to 8.5 MeV/c as they traversed the 29.4-cm-long hydrogen target.

The mass resolution shown in Fig. 4(a) was formed by using the Gaussian equivalents of the component contributions. This is an approximation and in order to extract the ω mass and width a full Monte Carlo simulation of the experiment and ω production was used. The program allowed for Landau fluctuations in the energy loss by ionization of the beam pions in the hydrogen target and a small amount of material upstream of it. Also included was a small extra timing error owing to different possible interaction points of the neutron in the neutron counter. Finally, a small non-Gaussian tail (affecting 9% of the events by typically 1 nsec) was added to the time-of-flight resolution to stimulate the effects of neutrons scattering off shield walls into the neutron counters. In view of

the uncertainty about this tail, we increased the errors on all the results to allow for ±100% changes in the size of the tail.

III. DATA COLLECTION

We initially intended to collect data at very low P^* by positioning a counter, N_7, on the beam axis 6.15 m downstream of the hydrogen target and inside the ring of six neutron counters N_{1-6}. However, N_7 gave a very high rate of accidental triggers. By various tests we were able to attribute most of these to μ^+ mesons which had been produced and stopped inside N_7, the subsequent electron decay producing the accidental coincidence. This also led to an increase in N_{1-6} accidentals. Therefore, we decided to collect the low-P^* data with N_7 in a separate series of runs. The N_7 accidental rate was reduced sufficiently by positioning it only 4.15 m from the target and operating with a beam intensity of 7×10^4 π's in the 200-msec spill (half the intensity used for the N_{1-6} data collection).

For the N_{1-6} data about 40 runs were taken, each corresponding to 6×10^8 π's spread over 5 adjacent momentum bins of 0.5% width. After each run the momentum was changed so that by scanning up and down a range of momentum from 0.935 to 1.319 GeV/c was covered, most of the data being concentrated near the ω threshold. A similar procedure was followed to obtain the N_7 data but the momentum interval covered was not as wide. The distribution of data as a function of P_π is shown in Fig. 5.

During the runs, the spectrometer bending-magnet field was monitored by observing an NMR signal, and found to be stable to within ±0.01%. The quadrupole currents were stable to within 0.1%. The spectrometer was sensitive to relative movements of the quadrupoles in the horizontal plane perpendicular to the beam axis. These movements were monitored by an optical system mounted above the magnets which was sensitive to movements changing the momentum scale by 0.003%, corresponding, for example, to a 10-μm shift in the $Q3$ position. It was found that restoring vacuum to the beam pipes after floating-wire measurements caused movement corresponding to a shift in momentum scale of ±0.06%. During the data-taking the effects were less than 0.02%. Floating-wire calibrations made before and after data-taking were consistent to within 0.01%, although the quadrupoles had moved such that a change of 0.03% was expected.

The photomultipliers of the beam-timing counter and neutron counters were voltage-stabilized to within ±1 V and, together with the electronics,

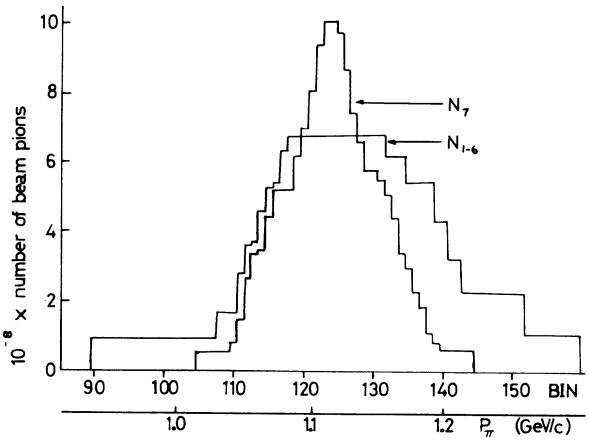

FIG. 5. The distribution with momentum of the total number of incident beam pions accumulated in the experiment.

were temperature-stabilized to within 1 °C. The neutron-counter gains were set so that their threshold bias was 7.9 ± 1.0 MeV electron equivalent. The gains and relative timing of the neutron counters were periodically checked and adjusted, and found to be stable to within ±2.5% and ±0.25 nsec, respectively. The timing scale was regularly calibrated, with the results being consistent to 0.05% and linear over the relevant range. The timing stability of each run was monitored by the width and position of the time-of-flight distribution of fast charged pions scattered from the beam. These were stable to within ±2% and 0.06 nsec, respectively.

The estimated neutron-counter efficiency varied smoothly from 23.5 to 25.5% over the relevant range of neutron energies. The efficiency was evaluated using the computer program of Stanton,[2] which was based on several experimental measurements of neutron-counter efficiencies, including some made by Crabb *et al.*[3] on counters almost identical to our own.

IV. RESULTS

A. The ω cross section

In deducing the ω cross section the decay array was used to select the $\pi^+\pi^-\pi^0$ channel. This improved the signal-to-background ratio by a factor of five, thus greatly reducing the effects on determinations of cross sections, M_ω or Γ_ω, of uncertainties in the background. The Monte Carlo simulation of the decay array indicated that the efficiency of the $\pi^+\pi^-\pi^0$ selection was independent of P^* over the range covered to within 1%. To check this, the ratio of the selected and unselected signals was studied as a function of P^* and no sig-

nificant variation was found, the mean efficiency being $48 \pm 1.5\%$. For the N_{1-6} data, the background under the ω signal was represented by a three-term polynomial which was well constrained by the wide mass range covered. However, for the N_7 data, a smaller mass range was covered and a two-term polynomial was used. The effect of this on the cross-section determination was shown to be negligible ($< 2\%$) by fitting the N_{1-6} data over this smaller mass range with a two-term polynomial.

As mentioned previously, the ω cross section can in principle be found directly from the area under the resonance signal. However, the cross sections we found implied a significant variation of $d\sigma/dt$ within the P^* intervals used for the yield curves for $P^* < 100$ MeV/c. Because of this, we deduced the cross sections by fitting the yield curves with Monte Carlo generated yield curves incorporating a cross-section behavior approximating that found in a preliminary analysis. This preliminary cross-section estimate was made by fitting the yield curves with those from a Monte Carlo simulation which had as input an isotropic angular distribution and a constant $d\sigma/dt$ (i.e., $\sigma \propto P^*$). The cross-section behavior as a function of P^* thus determined was then approximated by the straight lines shown in Fig. 6, and was incorporated into subsequent Monte Carlo fits to the yield curves which were used to find the final cross sections. The resulting cross section, divided by P^*, is shown as a function of P^* in Fig. 6. The generally good agreement with the straight lines of the first approximation indicates that no further iterations are required.

Our cross sections, σ, are actually values of $4\pi(d\sigma/d\Omega)$ measured at c.m. angles that change slowly as P^* changes. They are corrected for all known experimental losses and for all ω decay modes. In addition to the errors shown on the individual points there is a normalization error of about $\pm 8\%$ coming mainly from uncertainties in the absolute neutron-counter efficiency.

The values of P^* at which the cross sections are plotted are the peak values of the P^* distributions (as given by the Monte Carlo simulation) for the particular yield curves. The widths (FWHM) of the P^* distributions are shown as a function of P^* in Fig. 4(b). The nonzero widths arise partly from the finite angular range subtended by the counters.

Before proceeding to a discussion of the P^* behavior of the cross section we first consider the information that we have on the production angular distribution. Although we measure at only two slightly overlapping laboratory angular ranges, each corresponds to two c.m. angles distinguished by different neutron times of flight. So we have differential cross sections at two points near $\theta^* = 0^\circ$ and two near $\theta^* = 180^\circ$, where θ^* is the c.m. production angle. If only S and P waves are present in the final state, then the angular distribution can

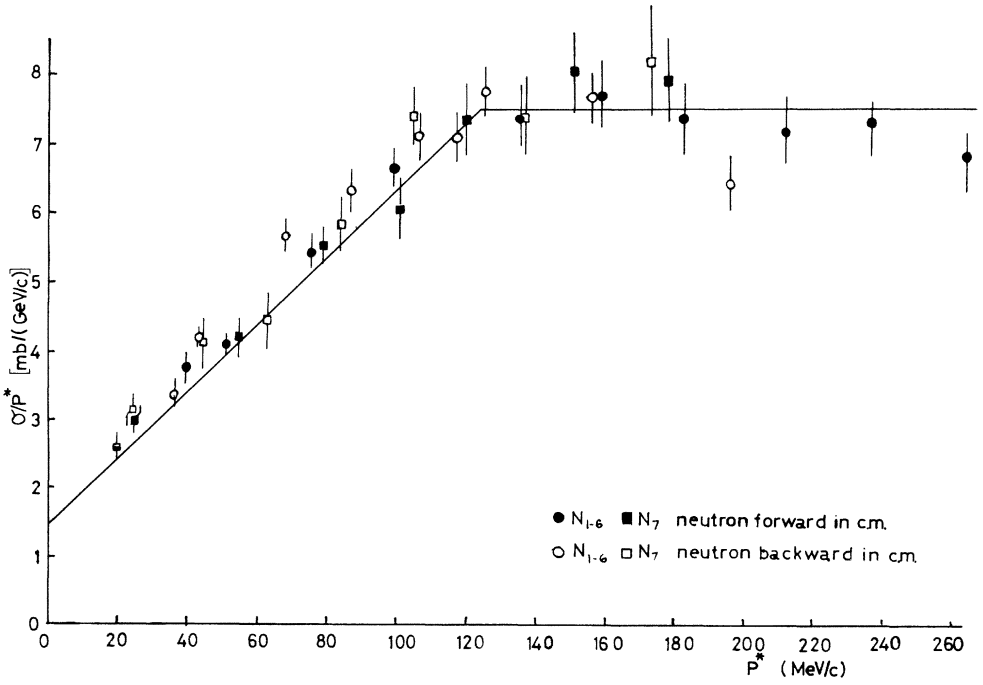

FIG. 6. The cross section σ/P^* as a function of P^*. The solid line is the shape of the cross section used in the Monte Carlo simulation.

be expanded in terms of Legendre polynomials as

$$a_0 + a_1 P_1(\cos\theta^*) + a_2 P_2(\cos\theta^*) \quad (1)$$

and we can therefore fit this expression to our four points to obtain a_0, a_1, and a_2 as functions of P^*. We can expect our determination of a_1 to be quite accurate since a_1 is essentially given by the difference of the forward and backward cross sections. However, it is only feasible for us to determine a_2 at very low P^* since, as P^* increases, our data become increasingly confined to small angular regions near 0° and 180°.

The results of the fits are shown in Fig. 7 and indicate that the $P_1(\cos\theta^*)$ term is consistent with zero and must in fact be very small. The $P_2(\cos\theta^*)$ coefficient is also consistent with zero but the limits we can put on it are not useful except at very low P^*.

Additional information about the ω angular distribution comes from the data of Abolins *et al.*[4] and Kraemer *et al.*[5] Both these experiments used a deuterium bubble chamber exposed to a π^+ beam. Each had approximately 100 events for a total c.m. energy <1800 MeV ($P^*<260$ MeV/c) and for this range neither experiment showed any evidence for a significant $P_2(\cos\theta^*)$ term. The data of Kraemer *et al.* showed a forward/backward asymmetry which was not apparent in the data of Abolins *et al.* and is strongly ruled out by our data (see Fig. 7). Taking all the evidence together, a reasonable conclusion is that the angular distribution is, in fact, isotropic to a good approximation. Thus, although we have covered only part of the full range of the c.m. production angle we feel it is justified at this stage to treat our values of σ as measurements of the total ω cross section.

The most striking feature of the cross-section points shown in Fig. 6 is the drop by a factor of 3 in σ/P^* between $P^*=120$ MeV/c and $P^*=20$ MeV/c. This confirms our earliest observation. We point out that the drop in cross section is not due to part of the yield curve being below the nominal ω threshold. This is because, by integrating over P_π, we always cover the full ω mass range even for the lowest P^* intervals (see Fig. 3). Neither could the effect be caused by variations in the neutron-counter efficiency since that was practically constant over the relevant range of neutron energies.

Figure 8 shows our cross section, σ, plotted as a function of P^* and also shows values from other experiments for the reaction $\pi^+ n \to \omega p$ which by isotopic-spin invariance should have the same cross section as $\pi^- p \to \omega n$. The agreement is satisfactory except at high P^* where the two experiments on $\pi^+ n \to \omega p$ disagree with each other by a factor of 2. As P^* increases above 200 MeV/c our isotropy

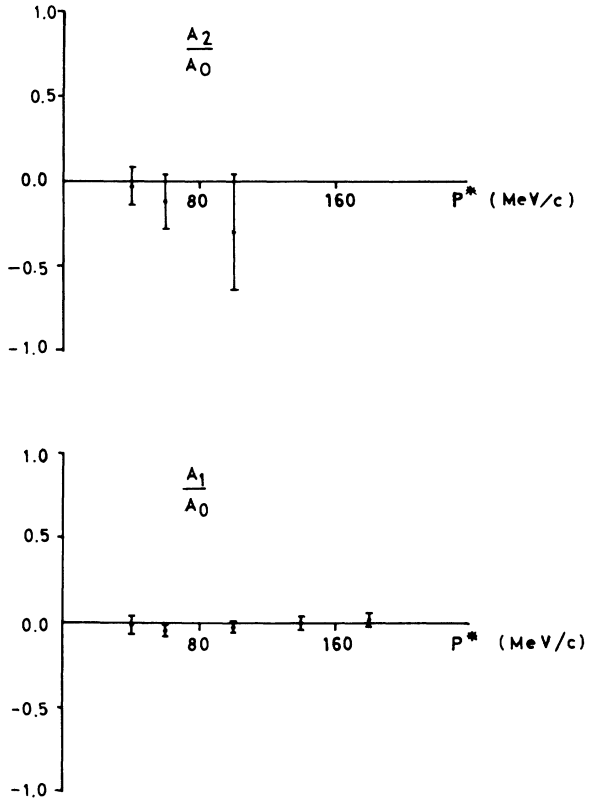

FIG. 7. The values of the ratios of the Legendre-polynomial coefficients from the fit to the angular distribution, as functions of P^*.

assumption becomes less reliable so that our cross sections there are of limited significance.

B. The ω mass

The best-fit values for M_ω for each of the P^* intervals used in the cross-section determination are shown as a function of P^* in Fig. 9(a). The errors shown are statistical only. The data do not show any evidence for a dependence of M_ω on P^*, in particular there is no change at very low P^*. The only systematic mass error that depends on P^* is that due to uncertainties in the absolute time-of-flight scale. If this were in error it would have almost no effect on the measured mass at low P^* since, to first order, that is independent of time of flight, but for larger P^* it would become significant, manifesting itself as an apparent difference between the ω masses deduced from neutrons produced forward and backward in the c.m. The limits we can deduce for this from our highest-P^* data [not shown in Fig. 9(a)] show that such an effect is negligible for $P^*<60$ MeV/c but that it could become comparable to the statistical error at $P^*=100$ MeV/c. For the N_7 data the effect

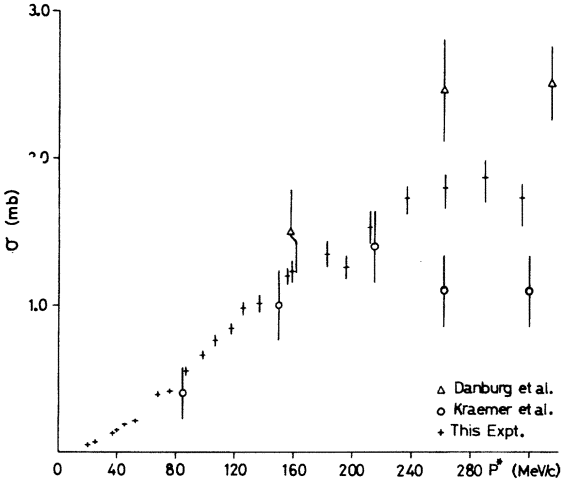

FIG. 8. The total cross section derived by assuming isotropy. The data shown for comparison are from the reaction $\pi^+ n \to \omega p$.

would be larger because of the shorter neutron flight path.

To obtain our best value for the ω mass we have used data from N_{1-6} alone in the interval from P^* = 55 MeV/c for forward neutrons in the c.m. to P^* = 60 MeV/c for backward neutrons in the c.m. approximately corresponding to the neutron time-of-flight interval 16–21 nsec. This choice avoids the use of data which might be affected by uncertainties in the absolute time-of-flight scale while maintaining good statistics (about 7 000 ω's above background). The $\pi^+\pi^-\pi^0$ yield curve for this P^* interval is shown in Fig. 10(b). A three-term polynomial was used to represent the background.

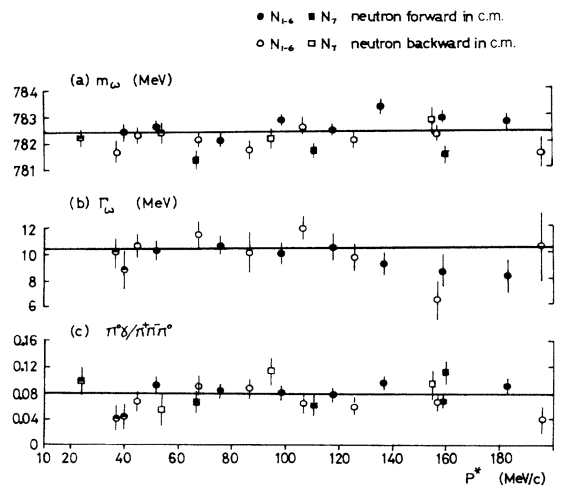

FIG. 9. Plots of (a) the mass, (b) the width, and (c) the branching ratio $\Gamma(\omega \to \pi^0\gamma)/\Gamma(\omega \to \pi^+\pi^-\pi^0)$ as functions of P^*. The horizontal lines represent our overall best values for these three quantities.

This fit gave the value $M_\omega = 782.4 \pm 0.16$ MeV (statistical error). Although this fit was good ($\chi^2 = 60$ for 66 degrees of freedom) we also tried fits with different-degree polynomials for the background. Any shift in mass was always less than 0.05 MeV. A shift in the measured mass could also be produced if the $\pi^+\pi^-\pi^0$ decay selection introduced a bias in the interaction point in the hydrogen target. Monte Carlo studies showed that any effect must be small as might be expected since the solid-angle coverage of the decay array is very large. This was checked by comparing the mass deduced for selected and unselected events. The mass shift observed was 0.24 MeV. We believe this discrepancy is mainly due to the effect of the large rapidly varying background in the unselected mass spectrum and hence we favor the value obtained from the $\pi^+\pi^-\pi^0$ yield curve (see Fig. 10). However, we have included a systematic error of ±0.25 MeV because of the possibility of a bias in

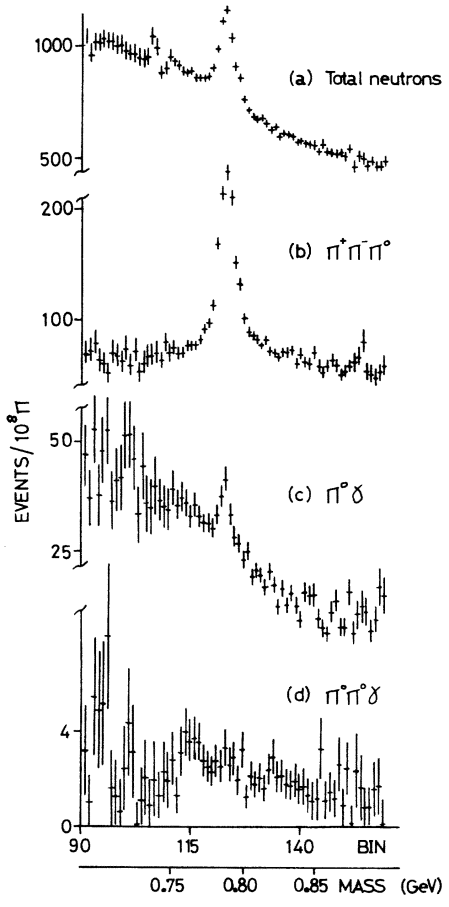

FIG. 10. N_{1-6} yield curves for a fixed P^* interval from 55 MeV/c (neutrons forward in c.m.) to 60 MeV/c (neutrons backward in c.m.) for various decay selections: (a) No decay selection; (b) $\pi^+\pi^-\pi^0$; (c) $\pi^0\gamma$; (d) $\pi^0\pi^0\gamma$. Note also the mass scale.

the $\pi^+\pi^-\pi^0$ selection.

The largest contribution to the systematic error comes from the uncertainty in the incident-momentum scale. The incident-momentum spectrometer was calibrated by means of the floating-wire technique in terms of standard units of mass, potential, and resistance. The dominant error in the calibration, ± 0.04%, came from the uncertainty in relating floating-wire measurements to the hodoscope-counter positions. An additional uncertainty in the momentum scale was caused by relative movements of the quadrupole beam elements whose positions were monitored by an optical system as described in Sec. III. We have assigned a systematic error of ±0.06% to this, corresponding to the maximum movement observed.

Since there are several independent components to the systematic error we have combined them quadratically with the statistical error to give a total error of 0.5 MeV (standard deviation). Thus our result for the ω mass is

$$M_\omega = 782.4 \pm 0.5 \text{ MeV}. \quad (2)$$

Since the uncertainties in our incident-momentum scale are the largest contribution to our total error in the ω mass we have attempted to check it by studying the reaction $\pi^- p \to K^+\Sigma^-$ at threshold, a reaction in which all the masses are accurately known and whose threshold is very close to that of $\pi^- p \to \omega n$. The K^+ was detected in the neutron counters and the π^- from the Σ^- decay was detected in the decay array. The resulting yield curve for 17 to 22 nsec is shown in Fig. 11. The fit to these data indicated that our mass scale was high (i.e., implied a lower ω mass) by 0.55 ± 0.25 MeV (statistical error only). However, there are several problems in the analysis. Because of decays, only 5% of the K^+'s reach the neutron counters, a comparable number of events being due to the detection of the μ^+ from the $K^+ \to \mu^+\nu$ decay. Also the ionization-energy loss of the K^+ depends upon the interaction point in the hydrogen target, which is biased by the detection of the π^- from the Σ^- decay. Finally, one cannot assume $\sigma \propto P^*$ since the particles are charged.[6] We estimate that these difficulties introduce a 0.5-MeV systematic error. Although this test is not significant enough to warrant changing our mass scale, it gives us confidence that our systematic error in M_ω is adequate.

Our result agrees with our previous determination[1] of M_ω and with the world average value[7] of 782.66 MeV (which includes the result of this paper). The experiments which contribute most significantly to the world average are listed in Table I (data are from Refs. 7–15 and our experiment). For several of them the error quoted is statistical only.

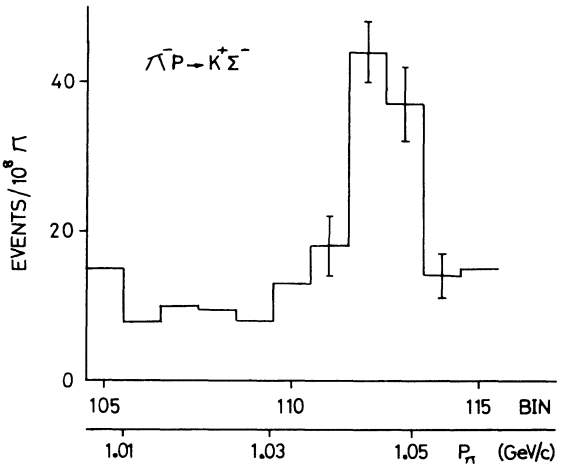

FIG. 11. The yield curve for the $K^+\Sigma^-$ channel with $P^* < 50$ MeV/c. Each bin corresponds to approximately 3 MeV in missing mass recoiling from the K^+.

The systematic mass error is *a priori* likely to be small in stopping $\bar{p}p$ experiments and we note that we are in good agreement with the mean of these experiments,[8-11] 782.1 ± 0.3 MeV. We also agree well with the 782.5 ± 0.8 MeV result of the $K^- p \to \Lambda\omega$ experiment of Aguilar-Benitez *et al.*,[13] which has a very good signal-to-background ratio and reasonable resolution. Finally, we note that Roos and Rousku,[16] in a recent compilation study of the ω mass, discuss the problems associated with systematic errors and obtain a best value of 783.4 ± 0.4 MeV (not including our result).

C. The ω width

The best-fit values for Γ_ω for each of the P^* intervals used in the cross-section determination are shown as a function of P^* in Fig. 9(b). The errors shown do not include systematic errors. There is no significant evidence for any dependence of Γ_ω on P^*. Since the mass resolution is best at low P^* and for neutrons produced backwards in the c.m. we used data in the interval from $P^* = 80$ MeV/c (forward-produced neutrons in the c.m.) to $P^* = 200$ MeV/c (backward-produced neutrons in the c.m.) to deduce our overall best value for Γ_ω. This represented the best compromise between the requirements of good statistics and good resolution and yielded a data sample with about 20 000 ω's above background and with a resolution function of 6.6 MeV FWHM. The value for Γ_ω for this data sample was 10.22 ± 0.35 MeV (statistical error).

The systematic error in Γ_ω comes mainly from uncertainties in the resolution. Our incident-momentum resolution was 0.50 ± 0.05% with the error coming from small uncertainties in the size and

TABLE I. A compilation of several significant measurements of M_ω and Γ_ω.

M_ω (MeV)	Γ_ω (MeV)	Resolution FWHM (MeV)	Signal to background	No. of ω's	Reaction	Momentum (GeV/c)	Detector technique	Reference
783.4 ±0.7	...	47	1	3221	$\bar{p}p \to \omega\pi^+\pi^-$	0.0	HBC	Baltay *et al.* (Ref. 8) (1967)
782.4 ±0.5	...	29	4	2400	$\bar{p}p \to \omega\pi^+\pi^-$	0.0	HBC	Bizzari *et al.* (Ref. 9) (1969)
784.0 ±0.7	11.2 ±2.7	...	1	2960	$\bar{p}p \to 3\pi^+\pi^-\pi^0$	3.6	HBC	Atherton *et al.* (Ref. 10) (1970)
783.4 ±1.0	12.8 ±3.0	≃8.5	≳20	248	$\bar{p}p \to K^+K^-\omega$	0.0	HBC	Bizzari *et al.* (Ref. 11) (1971)
781.0 ±0.5	10.3 ±1.4 [a]	5.4	≳20	510	$\bar{p}p \to K_1K_1\omega$	0.0	HBC	Bizzari *et al.* (Ref. 11) (1971)
783.7 ±1.0 [a]	9.5 ±1.0 [a]	b	≃10	b	$\pi^+p \to \pi^+p\omega$	3.7	HBC	Coyne *et al.* (Ref. 12) (1971)
782.5 ±0.8	13.3 ±2.0	16	10	418	$K^-p \to \Lambda\omega$	3.9	HBC	Aguilar-Benitez *et al.* (Ref. 13) (1972)
...	9.1 ±0.8	...	≳20	...	$e^+e^- \to \omega$	...	OSPK	Benaksas *et al.* (Ref. 14) (1972)
783.1 ±2 [c]	7.7 ±1.65 [c]	9.0	4	940	$\pi^-p \to \omega n$	2.5	MMS	Brown *et al.* (Ref. 15) (1972)
782.4 ±0.5 [a]	10.2 ±0.43 [a]	6.6 [d]	4	20 000	$\pi^-p \to \omega n$	threshold MMS		This experiment
782.66 ±0.32 [e]	9.98 ±0.38 [e]							Particle Data Group (Ref. 7)

[a] Systematic errors included (added quadratically).
[b] This experiment has a wide range of resolution, the mean being ≃30 MeV for the total number of events = 4268. There are 2309 events with resolution <23.5 MeV.
[c] Systematic errors included (added linearly).
[d] See Fig. 4(a).
[e] Includes our result, but with our error in Γ_ω being taken as 0.6 MeV.

position of the hodoscope counters and in the spectrometer focusing. We checked the momentum resolution by studying the η meson. Details are given in Ref. 1 and in Ref. 17. The timing resolution was determined from a study of fast neutrons from backward charge-exchange scattering and the reaction $\pi^-p \to \eta n$ at 725 MeV/c (considerably above the η threshold). It was found to have a standard deviation of 0.60 ± 0.05 nsec. After allowing for the uncertainty in the non-Gaussian tail in the time-of-flight distribution (see Sec. II), the total uncertainty in the mass resolution contributed 0.22 MeV to the uncertainty in the width measurement. A further contribution to the error comes from uncertainties in background shape. This was estimated by using a four- instead of a three-term polynomial and was found to be < 0.1 MeV. The systematic error in Γ_ω increases with P^* and exceeds the statistical error for $P^* > 120$ MeV/c for neutrons produced forwards in the c.m. For neutrons produced backwards it is of much less importance. This is the main reason for the restricted range of P^* used in the measurement of the best value of Γ_ω. Since there are several independent contributions to the error in the width, we consider that they should be added quadratically to the statistical error. Thus our value for the ω width is

$$\Gamma_\omega = 10.22 \pm 0.43 \text{ MeV}. \quad (3)$$

We note from Table I that the previous three most accurate measurements of the ω width, using very different techniques, gave results in reasonable agreement with the above value. The experiment of Coyne *et al.*,[12] a bubble-chamber study of $\pi^+p \to \pi^+p\omega$ at 3.7 GeV/c, had relatively poor resolution but adequate statistics. They quote their result as $\Gamma = 9.5 \pm 1.0$ MeV (9.2 ± 1.6 MeV if pessimistic). In the experiment of Benaksas *et al.*,[14] the ω width was determined by an excitation curve of e^+e^- collisions and their result (9.1 ± 0.8 MeV) was limited by statistics only. Bizzari *et al.*,[11] from a bubble-chamber study of $\bar{p}p$ annihilations at rest into $K\bar{K}\omega$, found $\Gamma = 10.3 \pm 1.4$ MeV. Their experiment had good resolution but limited statistics.

D. Effect of different line shapes on values of M_ω and Γ_ω

The spectra were fitted with a simple nonrelativistic Breit-Wigner shape convoluted with the experimental resolution function. Since the width of the resolution function was approximately half of the intrinsic width of the ω, it was the latter that dominated the shape. If the actual line shape of the ω is different from a nonrelativistic Breit-Wigner shape, then the value of Γ obtained from the fits

would correspond closely to the FWHM value of the actual line shape. This is because the points in the neighborhood of the half-maximum points are the most sensitive ones for M_ω and Γ_ω. Thus one can obtain an estimate of the possible effects by finding the difference, $\Delta\Gamma$, in FWHM value of a nonrelativistic Breit-Wigner shape and various other possible line shapes. Similarly, the effect on the fitted central mass can be estimated from the difference, ΔM, between the mean of the half-maximum points of a nonrelativistic Breit-Wigner shape and the various line shapes. We consider three modifications to a nonrelativistic Breit-Wigner shape and for each we evaluate $\Delta\Gamma$ and ΔM.

Relativistic Breit-Wigner shape:

$$f(M)=\frac{M_0^2\Gamma^2}{(M_0^2-M^2)^2+M_0^2\Gamma^2}\ , \tag{4}$$

$$\Delta\Gamma=\Gamma^3/8M_0^2=0.002\ \text{MeV},\qquad \Delta M=\Gamma^2/8M_0=0.017\ \text{MeV}. \tag{5}$$

Phase-space modified Breit-Wigner shape:

$$f(M)=\frac{\frac{1}{4}\Gamma^2}{(M_0-M)^2+\frac{1}{4}\Gamma^2}\ ,\quad \Gamma\propto 3\pi \text{ phase space}. \tag{6}$$

Near M_0 this gives $\Gamma=\Gamma_0+a(M-M_0)$, with $a\sim 0.05$. Then

$$\Delta\Gamma=\tfrac{1}{4}a^2\Gamma_0=0.006\ \text{MeV},\qquad \Delta M=\tfrac{1}{4}a\Gamma_0=0.12\ \text{MeV}. \tag{7}$$

Interference with a constant background:

$$f(M)=\left|\frac{\frac{1}{2}\Gamma}{(M_0-M)-\frac{1}{2}i\Gamma}+Ae^{i\theta}\right|^2. \tag{8}$$

For $A\ll 1$,

$$\Delta\Gamma=A^2\Gamma\cos^2\theta,\qquad \Delta M=A\Gamma\cos\theta. \tag{9}$$

Limits on $A\cos\theta$ can be deduced from the comparison we can make of the best-fit masses of the $\pi^+\pi^-\pi^0$ and $\pi^0\gamma$ decay modes since the latter should have a negligible coherent background. Our value for this mass difference is 0.3 ± 0.5 MeV, giving one-standard-deviation limits on ΔM of $-0.2<\Delta M<+0.8$ MeV and $-0.02<A\cos\theta<+0.08$ and hence $\Delta\Gamma<0.064$ MeV.

A more stringent limit on the interfering background amplitude was obtained by fitting the $\pi^+\pi^-\pi^0$ mass spectra with the above line shapes. This enabled us to deduce the limits $-0.02<A\cos\theta<0.01$ and hence

$$-0.2<\Delta M<+0.1\ \text{MeV},\qquad \Delta\Gamma<0.004\ \text{MeV}. \tag{10}$$

It can be seen that the above three line shapes produce a negligible perturbation to Γ_ω, but could produce a shift in the measured value of M_ω by about 0.2 MeV. Thus we see no reason to alter the best values or errors in our measurement of M_ω and Γ_ω.

E. The ω branching ratios

The "decay array" of scintillation counters around the target enabled us to select events according to the number of charged particles and γ rays in the final state and to make some simple cuts on azimuthal angles between particles to ensure consistency with transverse-momentum conservation. The decays we considered for the ω were $\pi^+\pi^-\pi^0$, $\pi^0\gamma$, and $\pi^0\pi^0\gamma$. We ignored the $\eta\gamma$ decay since this has been measured[18] to have a branching ratio of less than 6% of the $\pi^0\gamma$ decay. Also we were not able to measure the small $\pi^+\pi^-$ decay since we could not separate it clearly from $\pi^+\pi^-\pi^0$.

Our $\pi^+\pi^-\pi^0$ selection required two charged particles and two γ rays in the final state with some loose cuts on azimuthal separation. Our $\pi^0\gamma$ selection required three γ rays with the bisector of two of them being roughly opposite in azimuth to the third. The $\pi^0\pi^0\gamma$ selection required greater than three γ rays with additional requirements to ensure a low probability of $\pi^0\gamma$ decays simulating $\pi^0\pi^0\gamma$ decays, owing to one γ ray being detected in two counters for example. The efficiencies of these selections were determined by a Monte Carlo program which was based on measurements of the response of the counters to π's and γ's, including measurements made in a tagged photon beam. The program also took into account the effect of δ rays produced by beam pions. To check and refine the Monte Carlo program, we studied the response of the decay array to the reactions $\pi^-p\to\pi^0n$, $\pi^-p\to\pi^+\pi^-n$, and $\pi^-p\to\eta n$ at lower momentum. A further check was provided by comparing our computed efficiency for the $\pi^+\pi^-\pi^0$ decay with that deduced from the ratio of the ω cross section for selected and unselected events. The Monte Carlo program determined the $\pi^0\gamma$ selection efficiency to be $54\pm8\%$ and the $\pi^0\pi^0\gamma$ efficiency to be $9\pm2\%$. The simulation showed that there was no dependence on P^* of the $\pi^+\pi^-\pi^0$ and $\pi^0\gamma$ selection efficiencies.

The branching ratios were deduced by comparing the ω signal in yield curves for the above selections. No evidence was found for an ω signal in the $\pi^0\pi^0\gamma$ selection [see Fig. 10(d)]. This enables us to set an upper limit:

$$\frac{\Gamma(\omega\to\pi^0\pi^0\gamma)}{\Gamma(\omega\to\pi^0\gamma)}<0.18\quad(95\%\text{ confidence level}). \tag{11}$$

This is to be compared with the upper limit of 0.1 for this ratio set by Barmin *et al.*[19].

The $\pi^0\gamma$ selection was used to evaluate the ω cross section as a function of P^* for the $\pi^0\gamma$ decay mode in the same way as was described above for the $\pi^+\pi^-\pi^0$ decay. An example of a $\pi^0\gamma$ yield curve is shown in Fig. 10(c). Hence the $\pi^0\gamma/\pi^+\pi^-\pi^0$ branching ratio was found as a function of P^*. This is plotted in Fig. 9(c). Although the points do show some scatter, they are consistent with a constant value and there is no overall trend in them. Combining all our data gives the value:

$$\frac{\Gamma(\omega \to \pi^0\gamma)}{\Gamma(\omega \to \pi^+\pi^-\pi^0)} = 0.084 \pm 0.013. \quad (12)$$

The error is dominated by the systematic uncertainty in the $\pi^0\gamma$ selection efficiency. Our value for this branching ratio is in agreement with the previous two most accurate measurements: that of Baldin *et al.*,[20] who found 0.081 ± 0.020, and that of Benaksas *et al.*,[14] who found 0.109 ± 0.025. Also, Flatté *et al.*[21] determined the neutrals to the $\pi^+\pi^-\pi^0$ branching ratio to be 0.097 ± 0.016.

As stated before, our $\pi^+\pi^-\pi^0$ selection efficiency was deduced from a comparison of the ω signal seen in the $\pi^+\pi^-\pi^0$ selection with that seen with no decay selection and we used a value for the ω branching ratio ($\pi^+\pi^-\pi^0$/total) of 0.90 as given by the fit to ω decays performed in Ref. 7. Although the percentage uncertainty in this branching ratio is negligible compared with the other errors in our $\pi^0\gamma$ measurement, in order to be independent of this ratio we can quote our result as $\Gamma(\omega \to \pi^0\gamma)/\Gamma(\omega \to \text{total}) = 0.076 \pm 0.012$. Combining this with our value for Γ_ω of 10.22 ± 0.43 MeV gives the partial width $\Gamma(\omega \to \pi^0\gamma) = 0.78 \pm 0.13$ MeV.

V. DISCUSSION

The most striking feature of the data is probably the drop of nearly a factor of 3 in σ/P^* between $P^* = 120$ and 20 MeV/c. This confirms our original observation of this effect.[1] However, the present data have much greater accuracy and also extend down to lower values of P^* and we will therefore not consider the earlier data in this discussion. Note that while the individual points have been obtained for the 3π channel, checks at particular momenta have shown that this also reflects the behavior of the $\omega \to$ total cross section.

One of the original motivations of the experiment was to follow the ω behavior as the ω-neutron relative velocity was reduced until the average distance traveled before decay was within the range of the nuclear interaction. With a width of 10 MeV, the average separation of the ω and neutron at decay is equal to a pion Compton wavelength for $P^* = 31$ MeV/c. Two possible effects may then become significant for values of P^* in this region. Firstly, in analogy to collision broadening in atomic spectra, the ω decay could be modified by the proximity of the neutron as in the case of the $\Delta(1236)$ in π-deuteron scattering.[22] This would lead to an increase in Γ_ω at low P^*. We see no evidence for any such increase [Fig. 9(b)]. A second possible effect at low P^* could be a final-state interaction between the neutron and a π from the ω decay. This possibility was examined in some detail in Ref. 1 and could produce a drop in the cross section at low P^* similar to that which we find experimentally. However, such an effect would presumably be much stronger in the 3π than in the $\pi^0\gamma$ channel and so one would expect to see an increase in the $\pi^0\gamma$ branching ratio at low P^* which mirrored the fall in the $\pi^+\pi^-\pi^0$ cross section. No such increase is evident in Fig. 9(c). A final-state interaction might also distort the ω mass spectrum and again no such effect is seen. In fact, the general absence of any significant variation in the ω parameters other than σ/P^* is striking.

While detailed calculations of the effects of the ω decay have not been attempted, it now seems unlikely that they are of primary importance. We therefore look at the possibility that the production mechanism is responsible for the surprising cross-section behavior. Although an s-channel is more likely to be dominant close to threshold, and this will be considered below, it has been suggested to us that ρ exchange in the t channel could lead to the depression in σ/P^* near threshold because of the vanishing of the spin-flip term.[23] However, a detailed calculation shows that ρ exchange will produce a cross section near threshold of the form $d\sigma/d\Omega = AP^* + BP^*P_t^2$, where the second term is the spin-flip contribution, with A and B constants and P_t the transverse momentum. In our case, the transverse momentum is low throughout the range covered such that the second term is typically less than 3% of the first term. Even if the spin-flip term were to be significant, it would produce a marked forward/backward asymmetry in $(d\sigma/d\Omega)$ contrary to our data. So a ρ-exchange model can be completely rejected as an explanation for the observed cross-section behavior.

We therefore seek an alternative explanation in terms of s-channel partial-wave amplitudes. Now as $P^* \to 0$ the contribution to the cross section from a particular final-state orbital angular momentum L will behave as $\sigma/P^* \propto (P^*)^{2L}$, e.g., constant for $L = 0$, P^{*2} for $L = 1$, etc. Thus we have an *a priori* expectation that only S and P waves will be significant in our energy region. The rapid rise that we see in σ/P^* suggests that P waves are important.

However, some S wave is definitely required as the data on σ/P^* are inconsistent with a parabolic rise from zero.

The absence of a $P_1(\cos\theta^*)$ term in the angular distribution can be reconciled with the requirement for both S and P waves if the phase difference between them remains close to 90° throughout the range of P^* studied. This however, is not a necessary condition since there are several S- and P-wave amplitudes to be considered, some combinations of which are noninterfering. If we label amplitudes by $LL'(2S')(2J)$, where L and L' are the initial and final orbital angular momenta, S' is the final spin, and J is the total angular momentum, then the seven parity-conserving amplitudes with $L'=0$ or 1 and $L=0$, 1, 2, or 3 are ($SS11$), ($DS33$), ($PP11$), ($PP31$), ($PP13$), and ($FP35$). Of the possible S- and P-wave combinations, ($SS11$) + ($PP31$) and ($DS33$) + ($PP11$) lead to an isotropic angular distribution, while the combinations ($SS11$) + ($PP31$) + ($PP33$) + ($FP35$) and ($DS33$) + ($PP13$) + ($PP11$) produce no $P_1(\cos\theta^*)$ terms in the angular distribution although they do produce a $P_2(\cos\theta^*)$ term. Thus the possibility exists for there to be a substantial P-wave amplitude even if the angular distribution is isotropic.

With this in mind, we return to the problem of explaining the cross section as a function of P^*. We first consider whether S waves alone can provide an explanation. The rapid rise of σ/P^* is not consistent with a constant S-wave scattering length since that requires σ/P^* to *fall* slowly with P^*. However, it is conceivable that the rapid rise could be the manifestation of a narrow S-wave ωn resonance. We therefore tried to fit the cross sections with an S-wave Breit-Wigner resonance,

$$\sigma = \frac{\frac{2}{3}\pi\lambda^2(J+\frac{1}{2})\Gamma_{\pi p}\Gamma_{\omega n}}{(E-E_0)^2+\frac{1}{4}(\Gamma_{\pi p}+\Gamma_{\omega n}+\Gamma_0)^2}\ , \tag{13}$$

where E_0 is the resonance mass and $\Gamma_{\pi p}$, $\Gamma_{\omega n}$, and Γ_0 are its partial widths to the elastic, ωn, and all other channels, respectively. We put $\Gamma_{\omega n}=\gamma P^*$ where γ is constant and take $\Gamma_{\pi p}$ and Γ_0 as independent of energy. No reasonable fits could be obtained, the basic problem being that to achieve the rapid variation of σ at low P^* a small total width is required which would produce an almost equally rapid fall in σ/P^* above the peak. That this is clearly in conflict with the data can be seen in the dashed curve of Fig. 12, which is a fit to the data below $P^*=140$ MeV/c with an S-wave resonance. When the full range of our data is used in the fit the agreement at low P^* is very bad. Moreover, a narrow s-channel resonance near the ωn threshold would distort the ω mass spectrum and lead to a dependence of M_ω on P^* which is not observed. For example the S-wave resonance shown in Fig. 12 would lead to a variation with P^* of 2 MeV in the observed ω mass.

We therefore consider a combination of S and P waves. The threshold behavior of the P wave allows a rapid rise in σ/P^* at low P^* without leading to any distortion of the ω mass spectrum or any requirement for a rapid drop at higher P^*. We have assumed only one P-wave amplitude to be important and have parameterized it by a Breit-Wigner resonance as above. The symbols are defined as before but the partial width $\Gamma_{\omega n}$ now incorporates the Blatt-Weisskopf barrier factor[24]:

$$\Gamma_{\omega n}=\frac{\gamma P^*(RP^*)^2}{1+(RP^*)^2}\ . \tag{14}$$

The radius R was fixed at $1/m_\pi$. The S-wave contribution to σ was taken to be proportional to P^* (equivalent to a small S-wave scattering length). The sum of these two contributions gave equally good fits for $J=\frac{1}{2}$, $\frac{3}{2}$, and $\frac{5}{2}$. The result of the fit $J=\frac{1}{2}$ is shown in Fig. 12. The best-fit values of the parameters describing the Breit-Wigner resonance are: $E_0\simeq 1650$ MeV, $\Gamma_{\pi p}\simeq 200$ MeV, $\Gamma_0\simeq 100$ MeV, $\gamma=1.0$. The fitted curves for other J values are similar. The shape of the fitted curve is dominated by the barrier factor and there is uncertainty not only in the radius R which should be used but also in the formula for the barrier factor. Accordingly, the fitted values for the mass and width have limited significance and could be altered by about 100 MeV by comparatively small changes in the barrier factor.

The significance of our cross-section data seems to lie mainly in the fact that both S and P waves are required and that the P-wave contribution is surprisingly large, dominating over the S wave even very close to threshold. For example, at $P^*=160$ MeV/c, where σ/P^* attains its maximum value, the S-wave contribution to the cross section is 0.4 mb while the P-wave contribution is 0.85 mb. This large P-wave cross section is itself suggestive that there is a resonance close to the ωn threshold which couples to the P-wave ωn system. In considering which πp resonance could be responsible we need to refer back to the restriction that our angular distribution information places on the possible combination of amplitudes. If, as the evidence suggests, the angular distribution is isotropic, then the only allowed combinations of the amplitudes are ($SS11$) + ($PP31$) and ($DS33$) + ($PP11$). For both of these combinations the final-state P-wave component is linked to an initial πp state of $J=\frac{1}{2}$ and $L=1$. The nearest πp resonance with these quantum numbers is the $P11(1780)$. The difficulty is that it would be expected to feed both $PP31$ and $PP11$ amplitudes and so would lead to interference with a final-state S-

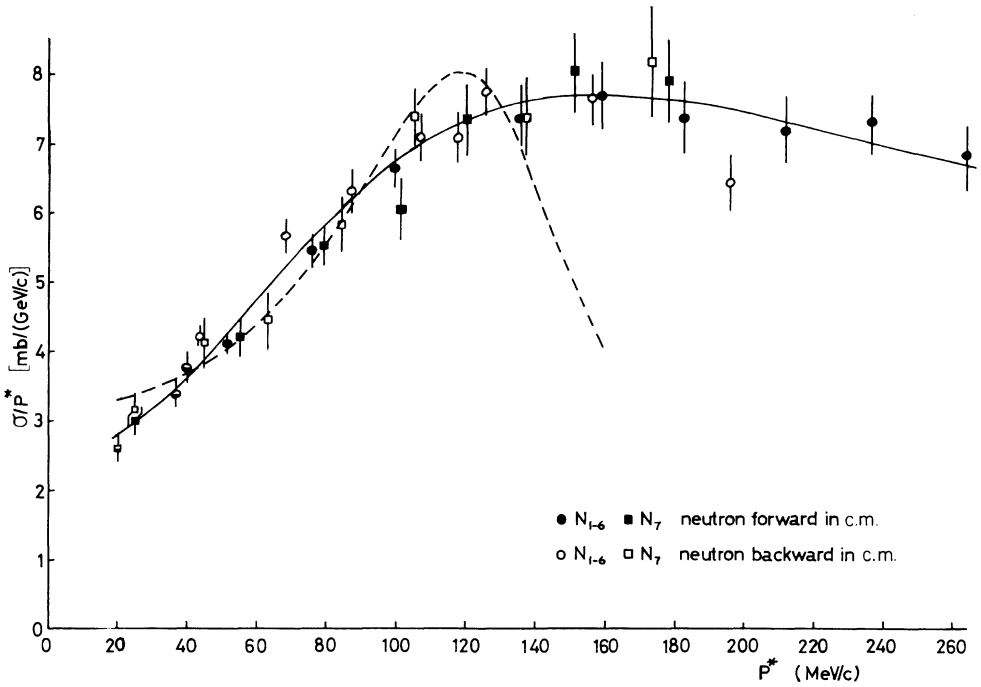

FIG. 12. The cross-section data fitted by models using an N^* to modulate the cross section. The broken curve shows an S-wave N^* fit for $P^* < 140$ MeV/c, the solid line is for a P-wave N^* plus a constant σ/P^* contribution.

wave amplitude. Thus, to maintain an isotropic angular distribution, one of the final-state P waves and one of the final-state S waves would have to be suppressed.

If we now allow a $P_2(\cos\theta^*)$ term to be present in the angular distribution but keep the prohibition on a $P_1(\cos\theta^*)$ term as our data require, then the initial πp state could be $L=1$, $J=\frac{3}{2}$ or $L=3$, $J=\frac{5}{2}$. The corresponding πp resonances which are nearby are the $P13(1810)$ and the $F15(1688)$. The $P13$ has the same difficulty as the $P11(1780)$, viz. the absence of a $P_1(\cos\theta^*)$ term requires the suppression of one of the amplitudes that the resonance can feed. However, the $F15(1688)$ can only produce a final-state $L'=1$ if $S'=\frac{3}{2}$, and so does not suffer from this difficulty. This can be taken as a point in favor of the identification of the $F15$ (1688) with the P-wave ωn state. A further point is that within the framework of an $SU(6)_W$ decay scheme for baryons, the ωn coupling of the $F15$ (1688) is predicted[25] to be considerably larger than that of the $P13(1810)$. However, the $F15$ would produce a large $P_2(\cos\theta^*)$ term in the angular distribution,[26] and while our data cannot rule this out they do suggest that it is unlikely. Thus none of the possible candidates for the large ωn P-wave cross section is completely satisfactory.

ACKNOWLEDGMENTS

We would like to thank R. F. Hobbs, D. G. Miller, and D. J. Scholes who carried out the mechanical design and construction of the apparatus and who helped us in many other ways. We also gratefully acknowledge the assistance of J. W. Hiddlestone and other staff of the Rutherford Laboratory.

[1]D. M. Binnie *et al.*, Phys. Rev. D 8, 2789 (1973).
[2]N. R. Stanton, Ohio State Univ. Report No. C00-1545-92, 1971 (unpublished).
[3]D. G. Crabb, J. G. McEwen, E. G. Auld, and A. Langsford, Nucl. Instrum. Meth., 48, 87 (1967).
[4]M. A. Abolins *et al.*, paper presented to the International Conference on High Energy Physics, Heidelberg, 1967 (unpublished). The $\cos\theta^*$ distribution for a different energy bin is shown by J. S. Danburg *et al.*, Phys. Rev. D 2, 2564 (1970).
[5]R. Kraemer *et al.*, Phys. Rev. 136, 496 (1964).
[6]E. P. Wigner, Phys. Rev. 73, 1002 (1948).
[7]Particle Data Group, Phys. Lett. 50B, 1 (1974).
[8]C. Baltay, J. C. Severiens, N. Yeh, and D. Zanello, Phys. Rev. Lett. 18, 93 (1967).
[9]R. Bizzari *et al.*, Nucl. Phys. B14, 169 (1969).

[10]H. W. Atherton *et al.*, Nucl. Phys. B18, 221 (1970).
[11]R. Bizzari *et al.*, Nucl. Phys. 827, 140 (1971).
[12]D. G. Coyne, W. R. Butler, G. Fang-Landau, and J. MacNaughton, Nucl. Phys. B32, 333 (1971).
[13]M. Aguilar-Benitez, S. U. Chung, R. L. Eisner, and N. P. Samios, Phys. Rev. D 6, 29 (1972).
[14]D. Benaksas *et al.*, Phys. Lett. 42B, 507 (1972); 42B, 511 (1972).
[15]R. M. Brown *et al.*, Phys. Lett. 42B, 117 (1972).
[16]M. Roos and J. Rousku, Helsinki Univ. Report No. ISBN 951-45-0326-0, 1974 (unpublished).
[17]A. Duane *et al.*, Phys. Rev. Lett. 32, 425 (1974).
[18]W. D. Apel *et al.*, Phys. Lett. 41B, 234 (1972).
[19]V. V. Barmin *et al.*, Zh. Eksp. Teor. Fiz. 45, 1879 (1963) [Sov. Phys.—JETP 18, 1289 (1964)].
[20]A. B. Baldin *et al.*, Yad. Fiz. 13, 758 (1971) [Sov. J. Nucl. Phys. 13, 431 (1971)].
[21]S. M. Flatté *et al.*, Phys. Rev. 145, 1050 (1966).
[22]D. V. Bugg, Nucl. Phys. B88, 381 (1975).
[23]We are grateful to R. Delbourgo for this suggestion and his calculation of the effect.
[24]J. M. Blatt and V. F. Weisskopf, *Theoretical Nuclear Physics* (Wiley, New York, 1956).
[25]R. J. Cashmore, A. J. G. Hey, and P. J. Litchfield, Nucl. Phys. B98, 237 (1975).
[26]A. Brandstetter, S. M. Deen, and P. J. Litchfield, Rutherford Laboratory Report No. RHEL/R 224, 1971 (unpublished).